Active tuned inerter-damper for smart structures and its $\mathcal{H}_\infty$ optimisation

G. Zhao [a,*], G. Raze [b], A. Paknejad [a], A. Deraemaeker [c], G. Kerschen [b], C. Collette [a,b]

[a] Université Libre de Bruxelles, Precision Mechatronics Laboratory, Beams Department, F.D.Roosevelt Av 50, 1050 Brussels, Belgium
[b] University of Liège, Department of Aerospace and Mechanical Engineering, Allée de la Découverte 9, 4000 Liège, Belgium
[c] Université Libre de Bruxelles, BATir Department, F.D.Roosevelt Av 50, 1050 Brussels, Belgium

ARTICLE INFO

ABSTRACT

In this paper, an active tuned inerter damper (ATID) is proposed and theoretically analysed. The proposed device is composed of a pair of collocated reactive actuator and force sensor. It is functioned by feeding back the output of the force sensor, through both single and double integrators to drive the actuator in order to destructively interfere with the host structure vibrations. The equivalent mechanical components for the single integrator and the double integrator are identified to correspond to a dashpot and an inerter, respectively. The $\mathcal{H}_\infty$ optimisation criterion is used for tuning the ATID, and closed-form expressions for the feedback gains are derived.

© 2019 Elsevier Ltd. All rights reserved.

1. Introduction

Tuned mass dampers (TMDs) have been widely used to suppress undesirable vibrations of various types of mechanical structures such as machinery, helicopters, bridges, buildings, etc. The most generic form of a TMD is an auxiliary system which consists of a proof mass and a spring-dashpot pair. The weight of the proof mass of TMDs is particularly important as it ultimately determines the vibration reduction performance of TMDs [1], where better control performance comes with a heavier proof mass. However, the added mass may be penalising in light weight applications, e.g. automotive and aerospace structures. In this context, the advantage of inerters is that their inertance can be significantly greater than their actual mass [2]. The inerter was initially proposed to complete the synthesis between the mechanical and electrical networks, where the effect of inerters on the dynamic behaviour of mechanical systems is designed to be similar to that of electrical capacitors in electrical systems [3]. It is defined as a one-port mechanical element which impedes the relative acceleration across its terminals [2,3]. Passive spring-damper-inerter systems have been studied mainly in the field of vibration isolation [4–6], and lead to a successful implementation in Formula One racing car suspension systems[3]. Inerter-based damper systems have also been proposed recently as an alternative to TMDs for passive vibration mitigation in [7], with the advantage that the realised equivalent mass ratio (inertance over primary structure mass) is greater than its actual mass ratio, leading to higher performance for the same effective mass. Alongside the applications for passive vibration damping and isolation, Zilletti [8] and Alujevic et al. [9] indicated that inerters can also be useful for further improvement of the performance of the traditional active vibration absorption and isolation systems in terms of the stability, robustness and vibration suppression capabilities. It was reported by Zhang et al. that the performance of nonlinear energy sinks in terms of vibration absorption can be further improved by integrating inerters into the design [10].

Several mechanical forms have been proposed to realise inerters in practice such as rack and pinion based inerters [2], ball and screw based inerters [3] and hydraulic inerters [11,12]. However, some imperfections due to the mechanical construction will be inevitably present preventing them to act as idealised inerters. For instance, the performance of rack and pinion and ball-screw inerters may degrade because of the friction and backlash or elastic effect of gears or screws [13], and hydraulic inerters may exhibit some nonlinear damping in addition to the inertance-like behaviour [11].

In order to address the aforementioned problems associated with passive inerters, the potential of using active tuneable inerter-dampers (ATID) has been investigated. Høgsberg et.al. [14] proposed to realise active inerter-damper systems using reactive actuators and force sensors. Reactive actuators are referred to as vibration actuators that are often used for smart structure applications, such as moving coil electrodynamic, magnetostrictive, piezoelectric, variable reluctance actuators, etc. They are typically embedded in the structures, which is different to inertial actuators where vibration actuators act against an inertial mass [15,16]. By feeding back the output of the force sensor through a resonant controller to derive the actuator, the proposed device behaves equivalently to a parallel connected inerter-damper-spring system. Another type of resonant controller, termed α controller, was investigated [17,18] for closing the loop between the force actuator and the force sensor, aiming to further improve the performance of the traditional active damping strategies, however the physics behind this controller was not yet fully interpreted. For both types of controllers, the corresponding controller parameters were optimised using the maximum damping criterion. In this paper, the α controller is simplified to a combination of a single integrator and a double integrator; the corresponding active device is shown to be dynamically identical to a serially connected inerter-damper pair. An $\mathcal{H}_\infty$ optimisation criterion is employed to derive the optimal parameters of the proposed ATID and the mechanical equivalent of the components in the proposed controller are explicitly discussed in order to provide more insights.

The paper is structured into 4 sections. Section 2 illustrates the working principle of the proposed ATID. In Section 3, the ATID is mounted into a single-degree-of-freedom (SDOF) system, based on which the closed-form optimal feedback gains for implementing the ATID are derived using the $\mathcal{H}_\infty$ optimisation criterion. Section 4 draws the conclusions.

2. Active tuned inerter-damper

The proposed ATID is schematically shown in Fig. 2(a). The system comprises a reactive actuator with its stiffness denoted by k_a and a collocated force sensor which measures the actual force, represented by F_s, transmitted to the structure. In this paper, idealised force sensors and reactive actuators are assumed where their internal dynamics are entirely neglected. The active control loop is implemented by feeding the output of the force sensor F_s through a controller $C(F_s)$ to drive the actuator which generates the resultant control force denoted by F_a:

$$F_a = C(F_s) = -g_s \int_0^t F_s dt - g_d \int_0^t \int_0^t F_s dt dt \tag{1}$$

where g_s and g_d represent the feedback gains of the single integrator the double integrator, respectively.

The governing equations of the ATID read:

$$F = -F_s \tag{2}$$

$$F_s = F_a - k_a \Delta x \tag{3}$$

where Δx represents the relative displacement between the two terminals of the device and F is the force applied on the ATID.

Substituting Eq. (1) into Eq. (3) and transforming the resulting equation into Laplace domain, one obtains,

$$Y(s) = \frac{\Delta V(s)}{F(s)} = \frac{s^2 + g_s s + g_d}{k_a s} = \frac{s}{k_a} + \frac{g_s}{k_a} + \frac{g_d}{k_a s} \tag{4}$$

where $Y(s)$ is defined as the driving point mobility of system seen from its terminals, $\Delta V(s)$ and $F(s)$ are the relative velocity and the applied force in the Laplace domain, and s represents the Laplace variable.

The moduli and phases of the driving point mobility of the ATID Y and its three dependencies are plotted in Fig. 1, where the following parameters are used, $k_a = 1$, $g_s = 1$ and $g_d = 100$. It can be seen that each individual term (from left to right) on the right hand side of Eq. (4) corresponds to the definition of the mobility of the mechanical element spring, damper and inerter respectively. This indicates that the proposed system with its port mobility defined by Eq. (4) can be alternatively realised by a pure mechanical network composed by a spring, a dashpot and an inerter connected in series. This equivalent mechanical scheme is shown in Fig. 2(b), where the equivalent damping coefficient d_a and the inertance m_a can be expressed by:

$$d_a = \frac{k_a}{g_s} \tag{5}$$

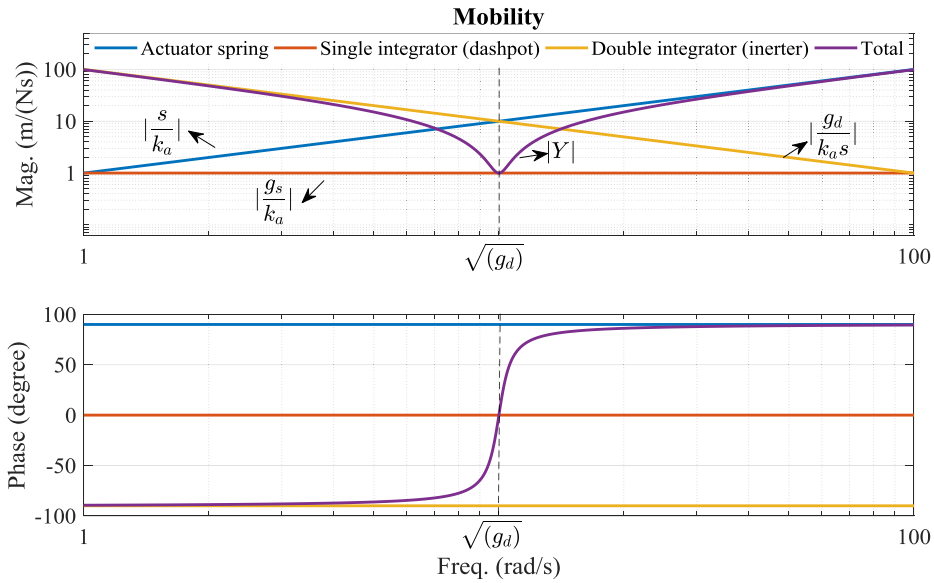$$m_a = \frac{k_a}{g_d} \tag{6}$$

Fig. 1. Mobility characteristics as a function of frequency for $k_a = 1$, $g_s = 1$ and $g_d = 100$.
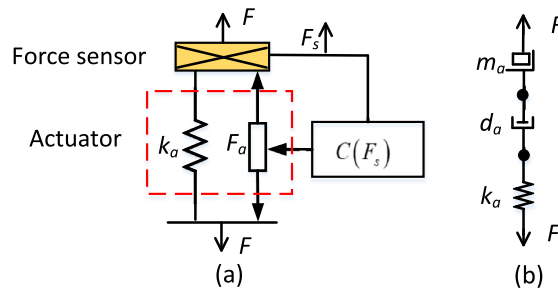

Fig. 2. (a) The scheme of the active tuned inerter damper and (b) its equivalent mechanical model.

Using Eqs. (5) and (6), the desired value of the equivalent damping and inertance can be obtained by adjusting the feedback gains g_s and g_d with respect to the actuator stiffness respectively.

It is also noted that the equivalent mobility of the ATID is frequency dependent. Below the frequency defined by $\sqrt{g_d}$ the ATID behaves similarly to an inerter whose inertance is determined by the feedback gain g_d as defined in Eq. (6). Above this frequency, it dynamics is dominated by the actuator spring. Around this frequency, an area is created where the ATID can impede the force transmission over its terminals and the minimal value of the modulus of Y is determined by the feedback gain g_s.

Moreover, it is also worth investigating the dynamic behaviour of the proposed ATID for some specific situations:

- both g_s and g_d are set to zero (corresponding to no control), there will be no relative displacement over d_a and m_a so that k_a represents the whole branch and the resultant system behaves as a spring;
- when the condition $g_s = 0$ and $g_d \neq 0$ is established, the ATID can be considered as an inerter-spring system. At its resonance frequency, the total mobility will be equal to zero as shown in Fig. 1, meaning that there is no relative motion transmitted through the system regardless of the applied force. For harmonic disturbance suppression, such a system can be useful as it introduces an anti-resonance in the coupled system, like the inductance shunt circuit to piezoelectric systems [19];
- on the other hand, when $g_s \neq 0$ and $g_d = 0$, the system becomes a dashpot and a spring connected in series, which is also known as a relaxation damper. This system can provide vibration suppression over a broad frequency band;
- finally, when at least one of the feedback gains approaches infinity, the mobility of the ATID is infinity (the corresponding impedance is zero) and no force is transmitted through this port element.

3. $\mathcal{H}_\infty$ optimisation of active tuned inerter-damper

An undamped, lumped parameter SDOF system as shown in Fig. 3(a) is employed to illustrate how to tune the proposed ATID to reduce certain vibration metrics in the frequency band of interest. Its equivalent mechanical network is depicted in Fig. 3(b). The SDOF system is defined through the mass m_1 and the suspension stiffness k_1. It is excited by a disturbance force F. The ATID is placed in parallel with the passive spring k_1.

The dynamic equations of the system in Fig. 3(a) are given:

$$m_1\ddot{x} + k_1 x = F + F_s \tag{7}$$

$$F_s = F_a - k_a x \tag{8}$$

In order to come to a more general formulation, the following parameters are introduced to normalise the system governing equations:

$$\tau = \omega_1 t, \quad x_1 = x, \quad x_2 = \int_0^t \int_0^t F_s dt dt / m_1, \quad x_d = F/k_1,$$
$$\omega_1 = \sqrt{\frac{k_1}{m_1}}, \quad \mu = \frac{k_a}{k_1}, \quad g^{sn} = \frac{g_s}{\omega_1}, \quad g^{dn} = \frac{g_d}{\omega_1^2} \tag{9}$$

Substituting Eqs. (1) and (9) into Eqs. (7) and (8), the equations of motion with the normalised parameters read:

$$x_1'' + x_1 - x_2'' = x_d \tag{10}$$

$$x_2'' + g^{sn} x_2' + g^{dn} x_2 + \mu x_1 = 0 \tag{11}$$

The $\mathcal{H}_\infty$ optimisation criterion is employed to optimise the ATID aiming to minimise the maximum magnitude of the frequency response of the system under consideration. In this context, the magnitude of the normalised driving point receptance $|x_1/x_d|$ is taken as the performance index.

The normalised driving point receptance of the primary structure is calculated as:

$$\frac{x_1}{x_d} = \frac{s^2 + g^{sn} s + g^{dn}}{s^4 + g^{sn} s^3 + (\mu + g^{dn} + 1)s^2 + g^{sn} s + g^{dn}} \tag{12}$$

and the modulus of its frequency response function reads,

$$\left|\frac{x_1}{x_d}\right| = \frac{\sqrt{\Omega^4 + \left((g^{sn})^2 - 2g^{dn}\right)\Omega^2 + (g^{dn})^2}}{\sqrt{\Omega^8 + \left((g^{sn})^2 - 2g^{dn} - 2\mu - 2\right)\Omega^6 + \left(-2(g^{dn})^2 + (-2\mu - 2)g^{dn} + (g^{sn})^2\right)\Omega^2 + \left((g^{dn})^2 + (2\mu + 4)g^{dn} + \mu^2 - 2(g^{sn})^2 + 2\mu + 1\right)\Omega^4 + (g^{dn})^2}} \tag{13}$$

where $\Omega = s/j$ is the normalised frequency.

As seen from Eq. (12), the control effectiveness of ATID is similar to that of a tuned mass damper from the mathematic point of view, where an additional zero is introduced to destructively interfere with the dynamics of the primary system. Following the $\mathcal{H}_\infty$ optimisation procedure, also known as the fixed point method, proposed by Den Hartog [1], the parameters of ATID are optimally tuned such that the responses at the fixed points are minimised. Fixed point refers to the frequency at which the magnitude of the driving point receptance of the primary structure is invariant in terms of the damping coefficient of the tuned mass damper or the control parameter g^{sn} for ATID.
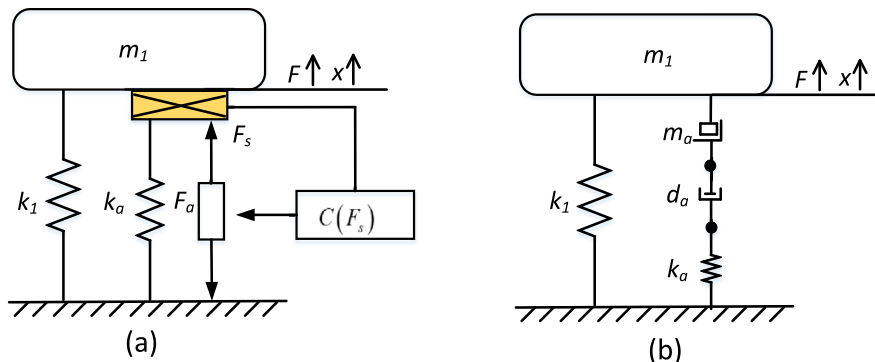

Fig. 3. (a) The scheme of the system under investigation and (b) its equivalent mechanical model.

The frequencies at which the fixed points occur can be calculated by differentiating Eq. (13) with respect to the damping coefficient, g^{sn}, and equating the derivative to zero, which yields:

$$\Omega_{f1} = \frac{\sqrt{\sqrt{4(g^{dn})^2 + (4\mu - 8)g^{dn} + (\mu + 2)^2} + 2g^{dn} + \mu + 2}}{2} \tag{14}$$

$$\Omega_{f2} = \frac{\sqrt{-\sqrt{4(g^{dn})^2 + (4\mu - 8)g^{dn} + (\mu + 2)^2} + 2g^{dn} + \mu + 2}}{2} \tag{15}$$

$$\Omega_{f3} = 0 \tag{16}$$

In fact, the fixed point Ω_{f3} only exists for the cases when at least one of the two feedback is non-zero and it can be neglected during the $\mathcal{H}_\infty$ optimisation process as it is basically invariant with respect to the parameters of ATID. The optimal g^{dn} is thus set to equalise the resulting performance index as defined in Eq. (13) at the first two fixed points. This can be done by substituting Eqs. (14) and (15) into Eq. (13) and equating the resulting expressions for $g^{sn} = 0$, one obtains,

$$g^{dn}_{opt} = 1 - \frac{\mu}{2} \tag{17}$$

For the optimal g^{sn}, it is sought to make the performance index horizontally pass through the fixed points. Thus, two optimal damping coefficients associated with the two fixed points are obtained:

$$g^{sn}_{opt1} = \sqrt{\frac{\mu\left(3\sqrt{2} - \sqrt{\mu}\right)}{2\sqrt{2}}} \tag{18}$$

$$g^{sn}_{opt2} = \sqrt{\frac{\mu\left(3\sqrt{2} + \sqrt{\mu}\right)}{2\sqrt{2}}} \tag{19}$$

The optimal g^{sn} can be taken in practice by calculating the quadratic average of Eqs. (18) and (19), which is given by:

$$g^{sn}_{opt} = \sqrt{\frac{\left(g^{sn}_{opt1}\right)^2 + \left(g^{sn}_{opt2}\right)^2}{2}} = \sqrt{\frac{3\mu}{2}} \tag{20}$$

It should be noted that this approach is an empirical method as the resulting resonance points (the derivative of Eq. (13) with respect to Ω is equal to zero) do not necessarily coincide simultaneously with the corresponding fixed points. An exact solution for this problem was proposed in [20], with which the two resulting resonance points are equally damped. In this study this exact approach is not considered because this would result in very long and therefore rather impractical polynomial expressions.

Up to now, only the stiffness ratio μ is left un-optimised. The influence of the stiffness ratio μ to the performance index $|x_1/x_d|$ can be assessed by evaluating its response at the fixed points. This is carried out by substituting Eqs. (14) and (17) or Eqs. (15) and (17) into Eq. (13) for $g^{sn} = 0$, yielding the minimal maximum response:

$$\left|\frac{x_1}{x_d}\right|_{opt} = \sqrt{\frac{2}{\mu}} \tag{21}$$

As shown in Eq. (21), the response at the fixed points is inversely proportional to the stiffness ratio μ, indicating that a stiffer ATID is preferred in practice in order to achieve a better control performance. However the maximum value of μ is limited by the constraint posed by Eq. (17), where the condition $\mu \leq 2$ should be valid in order to have a positive optimal feedback gain g^{dn}. This constraint can be better understood by looking at the evolution of the fixed point frequency Ω_{f2} defined by Eq. (15), which is feedback gain g^{dn} and stiffness ratio μ dependent. Substituting the optimal value of g^{dn} given by Eq. (17) into Eq. (15), it is noted that Ω_{f2} shifts to Ω_{f3} from the right hand side as μ approaches 2 from the left hand side and the two fixed points merge together at the zero location for any value of μ that is greater than 2. In such a scenario, there is only one tunable fixed point left which is located at Ω_{f1}. Although the performance index at this fixed point Ω_{f1} can be still further reduced, for example smaller than one, if a stiffer ATID is chosen as predicted by Eq. (21), this minimised maximum is no longer a global one as the value of the performance index at zero frequency remains equal to one. Therefore, for the cases where the stiffness of the ATID is greater than two times that of the passive spring, it is not necessary to include a double integrator into the controller $C(F_s)$ as a single integrator is already enough in the $\mathcal{H}_\infty$ norm sense to make the global minimal maximum to one.

In practice, transducers with high stiffness, such as piezoelectric stack actuators, magnetostrictive actuators or electromagnetic actuators with large guiding stiffness, are preferred as this would allow for the achievement of a better control

performance as illustrated in the text. However, it should be argued that much more force would be then transmitted through the actuator in this case which might not be favoured in practice because of the potential failure problem.

In addition, the stiffness ratio μ can be also calculated by:

$$\mu = \frac{\omega_0^2}{\Omega_0^2} - 1 \tag{22}$$

where ω_0 and Ω_0 correspond to the resonance frequencies of the system when the actuator is installed and removed respectively. In practice, ω_0 can be alternatively obtained by setting both feedback gains to zero and Ω_0 by setting either one of the two gains to infinity. In this context, the condition $\mu = 2$ leads to a shift of the resonance frequency by $\sqrt{3}$ times.

Although the optimal feedback gains given in Eqs. (17) and (20) are derived for a SDOF system, they can be also directly applied to multi-degree-of-freedom systems with well-separated modes in a manner analogous to classical TMDs [1] or piezoelectric shunts [21] using the modal information. For example, the stiffness ratio between the actuator and primary structure for a specific structural mode can be calculated by substituting the resonance frequencies associated with this mode when the control gains are set to zeros and infinity into Eq. (22). Afterwards, the optimal feedback gains can be obtained using the modal stiffness ratio.

Considering that the proposed ATID is an active system, its stability needs to be addressed. Although it is guaranteed because of its full analogy with a mechanical network given idealised force sensors and actuators are employed, it is not clear what are the gain and the phase margins of the system if the optimal feedback gains are used. In the forthcoming part, the open loop gain of the active system $L = G(j\Omega)C(j\Omega)$ is derived to study these margins. $G(j\Omega)$ and $C(j\Omega)$ represent the frequency response of the dimensionless sensor-actuator open loop transfer function and that of the dimensionless controller respectively, which are expressed as:

$$G(j\Omega) = \frac{1 - \Omega^2}{1 + \mu - \Omega^2} \tag{23}$$

$$C(j\Omega) = \frac{g^{sn}}{j\Omega} - \frac{g^{dn}}{\Omega^2} \tag{24}$$

Substituting the optimal settings of g^{sn} and g^{dn} as given in Eq. (20) and Eq. (17) into Eq. (24), one obtains:

$$L = \left(\frac{1 - \Omega^2}{1 + \mu - \Omega^2} \right) \left(\frac{1}{j\Omega} \sqrt{\frac{3\mu}{2}} - \frac{2 - \mu}{2\Omega^2} \right) \tag{25}$$

Fig. 4 plots the frequency response function of the open loop gain L as defined in Eq. (25) for four different stiffness ratios $\mu = 0.1$, $\mu = 0.5$, $\mu = 1$ and $\mu = 1.5$. It shows that the phase margin increases with an increase in the stiffness ratio μ. Thus, a greater value of the ratio μ is preferred for better robustness in terms of the phase margin. For the case $\mu = 0.1$, the phase margin is around 20°, and it is increased to 70° for $\mu = 1.5$. As the phase of the open loop gain is bounded between $-180°$ and $180°$, the gain margin of the ATID is infinite. This also proves that the closed-loop system is unconditionally stable.
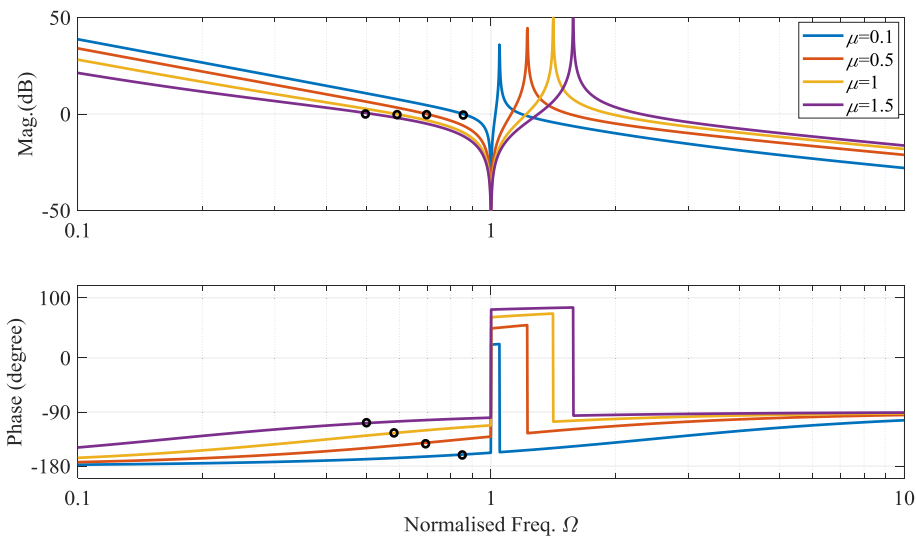

Fig. 4. Frequency response of the open loop gain L under the optimal feedback gains: unit gain crossover points (below the first anti-resonance frequency) are represented by circle points.

In the following, numerical studies are performed to illustrate the control effectiveness of the ATID for the system. Fig. 5 shows the performance index $|x_1/x_d|$ plotted against frequency for five different damping ratios defined as g^{sn}/g^{sn}_{opt}: 0, 1/4, 1, 4 and ∞, where the normalised gain for the double integrator g^{dn} is set to its optimal value given in Eq. (17) and the stiffness ratio μ is set to 0.2. It can be seen that all the curves with different damping values intersect at two frequencies and only with the optimal damping the response at the two fixed frequencies becomes maximum.

Fig. 6 compares the performance index $|x_1/x_d|$ for five additional cases. In the first three cases, the stiffness ratio μ is set to 0.01, 0.1 and 1, respectively and the control parameters g^{dn} and g^{sn} are updated for each case with their optimal values given by Eq. (17) and Eq. (20). As can be seen, the performance index $|x_1/x_d|$ indeed decreases with an increase in the stiffness ratio as indicated by Eq. (21). With this respect, the parameter μ can be understood to play the same role as the mass ratio of tuned mass dampers, where better performance comes with a greater value of this quantity. For the fourth case $\mu = 3$, the control parameters g^{dn} is set to 0 and g^{sn} is tuned according to Eq. (18). It is seen that the global minimal maximum is located at zero frequency instead of that at the fixed point given in Eq. (14) as discussed earlier in the paper. For the cases where μ is greater than 2, the minimal maximum at the fixed point degrades to a local maximum. Two other benchmarks are also included where the performance index $|x_1/x_d|$ is plotted for the following parameters: (i) $g^{sn} \to \infty$, $g^{dn} = 0$ and $\mu = 1$, and (ii) $g^{sn} = 0$, $g^{dn} = 0$ and $\mu = 1$, respectively. It is shown that the original undamped system with no control ($g^{sn} = 0$ and $g^{dn} = 0$) becomes undamped again when the feedback gain g^{sn} is set to infinity but with a shift of the resonance frequency. This is because for case (i) the impedance of the ATID is equal to zero such that no force will pass through the ATID as if it is
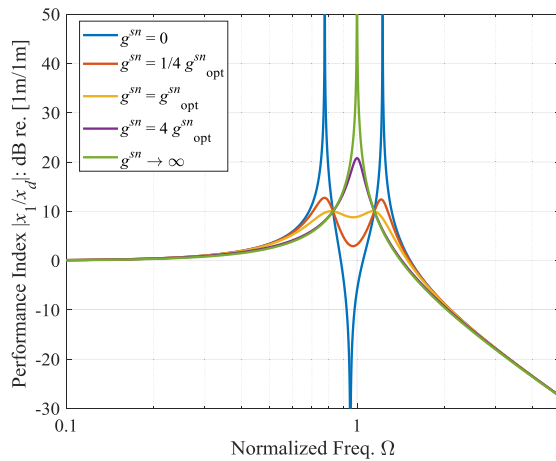

Fig. 5. The normalised driving point receptance for different values of the feedback gain g^{sn} where g^{dn} is set to its optimal value given in Eq. (17) and μ to be 0.2.
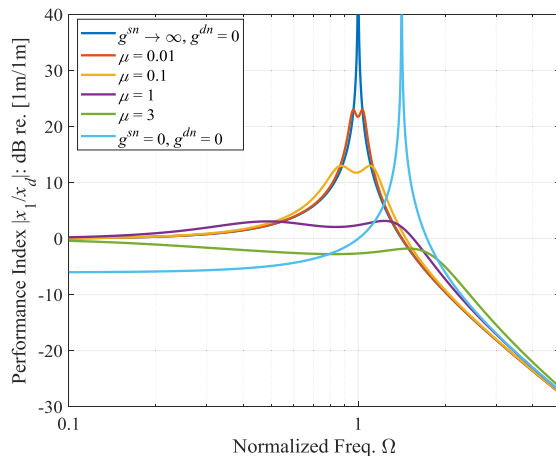

Fig. 6. The normalised driving point receptance for different values of μ where g^{dn} is set to its optimal value given in Eq. (17) and g^{sn} to Eq. (20), as well as two benchmarks where $g^{sn} \to \infty$, $g^{dn} = 0$ and $\mu = 1$, and $g^{sn} = 0$, $g^{dn} = 0$ and $\mu = 1$, respectively.

removed from the system, while for case (ii) the ATID degrades to a spring causing the increase in the resonance frequency. In addition, one should also notice that the system becomes dynamically softer with the use of the ATID when at least one of the feedback gains is set to non-zero values. This is caused by the fact that the installation of the ATID does not contribute to the static stiffness of the system. Chesné et.al. [18] proposed to include a high pass filter to the controller to compensate for the loss of the static stiffness. By doing so, it also facilitates the practical implementation of the ATID as over-amplifications of low frequency signals due to the use of the integrators could be avoided. However, its unconditional stability property is compromised as illustrated in [18].

Finally, the possible applications for the proposed device—Active Tuned Inerter-Damper should be stressed, which are mainly twofold: 1) for the inerter community: providing an alternative approach for the implementation of inerter-damper devices, which were mainly realised passively; 2) for the active damping community: promoting the employment of the proposed active controller over the classical IFF controller. The difference between the IFF controller and the proposed controller can be better illustrated with Fig. 2, where a relaxation damper is realised if IFF control (one single integrator) is applied while an inerter-damper (one single integrator and one double integrator) is realised if the apposed controller is applied. With the introduction of the inerter (double integrator), the control performance is improved in terms of suppression of vibration resonances compared to that with IFF controllers as it introduces an anti-resonance to the primary structure allowing a better interaction between the actuator and the primary structure as shown in Fig. 1. Moreover, the outperformance of the proposed controller is more pronounced for cases when soft actuators are used (the ratio between the actuator stiffness and the structure stiffness in the modal sense for a specific structural mode is low). This is in fact in a manner analogous to tuned mass dampers and relaxation dampers, or resistance-inductance shunts and resistance shunts for piezoelectric structures.

4. Conclusion

This paper discusses an active inerter-damper system which can be realised using a pair of collocated reactive actuator and force sensor. The corresponding controller consists of a single integrator and a double integrator. The equivalent mechanical models of the controller's components are derived in order to better illustrate the coupling of the electrical controller with the mechanical system. Closed-form expressions are derived using the $\mathcal{H}_\infty$ optimisation criterion wherein the optimal feedback gains are achieved to minimise the maximal response of the driving point receptance of the system under consideration. It is shown that the control effectiveness of the ATID is similar to that of a TMD. The performance of TMDs is mainly limited by their proof mass while the performance of ATIDs is governed by their stiffness. For practical implements, a stiffer ATID is preferred also for the robustness considerations in terms of the phase margins. For the cases when the stiffness of the ATID is greater than two times of the passive spring of the host structure in the modal sense, it might not be necessary to include a double integrator into the active controller $C(F_s)$ as a single integrator is already enough to achieve the same control performance in terms of the $\mathcal{H}_\infty$ norm. Also, it would be feasible in practice to develop a collocated actuator-force sensor pair together with the corresponding analogue electronic system in a compact fashion oriented for smart structure applications.

Acknowledgements

References

[1] J.P. Den Hartog, Mechanical Vibrations, Dover Publications, 1985, http://books.google.be/books?id=-Pu5YlgY4QsC.
[2] M.C. Smith, Synthesis of mechanical networks: the inerter, IEEE Trans. Automat. Contr. 47 (2002) 1648–1662, https://doi.org/10.1109/TAC.2002.803532.
[3] M.Z.Q. Chen, C. Papageorgiou, F. Scheibe, F.C. Wang, M. Smith, The missing mechanical circuit element, IEEE Circuits Syst. Mag. 9 (2009) 10–26, https://doi.org/10.1109/MCAS.2008.931738.
[4] J.Z. Jiang, A.Z. Matamoros-Sanchez, R.M. Goodall, M.C. Smith, Passive suspensions incorporating inerters for railway vehicles, Veh. Syst. Dyn. 50 (2012) 263–276, https://doi.org/10.1080/00423114.2012.665166.
[5] Y. Hu, M.Z.Q. Chen, Z. Shu, L. Huang, Analysis and optimisation for inerter-based isolators via fixed-point theory and algebraic solution, J. Sound Vib. 346 (2015) 17–36, https://doi.org/10.1016/j.jsv.2015.02.041.
[6] E. Sabbioni, A. Cigada, H.R. Karimi, A. Siami, E. Zappa, Parameter optimization of an inerter-based isolator for passive vibration control of Michelangelo's Rondanini Pietà, Mech. Syst. Signal Process. 98 (2017) 667–683, https://doi.org/10.1016/j.ymssp.2017.05.030.
[7] I.F. Lazar, S.A. Neild, D.J. Wagg, Using an inerter-based device for structural vibration suppression, Earthq. Eng. Struct. Dyn. 43 (2014) 1129–1147, https://doi.org/10.1002/eqe.2390.
[8] M. Zilletti, Feedback control unit with an inerter proof-mass electrodynamic actuator, J. Sound Vib. 369 (2016) 16–28, https://doi.org/10.1016/j.jsv.2016.01.035.
[9] N. Alujević, D. Čakmak, H. Wolf, M. Jokić, Passive and active vibration isolation systems using inerter, J. Sound Vib. 418 (2018) 163–183, https://doi.org/10.1016/j.jsv.2017.12.031.
[10] Y.-W. Zhang, Y.-N. Lu, W. Zhang, Y.-Y. Teng, H.-X. Yang, T.-Z. Yang, L.-Q. Chen, Nonlinear energy sink with inerter, Mech. Syst. Signal Process. 125 (2019) 52–64, https://doi.org/10.1016/j.ymssp.2018.08.026.
[11] S.J. Swift, M.C. Smith, A.R. Glover, C. Papageorgiou, B. Gartner, N.E. Houghton, Design and modelling of a fluid inerter, Int. J. Control. 86 (2013) 2035–2051, https://doi.org/10.1080/00207179.2013.842263.

[12] X. Liu, J.Z. Jiang, B. Titurus, A. Harrison, Model identification methodology for fluid-based inerters, Mech. Syst. Signal Process. 106 (2018) 479–494, https://doi.org/10.1016/j.ymssp.2018.01.018.

[13] C. Papageorgiou, N.E. Houghton, M.C. Smith, Experimental testing and analysis of inerter devices, J. Dyn. Syst. Meas. Control. 131 (2009), https://doi.org/10.1115/1.3023120 011001.

[14] J. Høgsberg, M.L. Brodersen, S. Krenk, Resonant passive – active vibration absorber with integrated force feedback control, Smart Mater. Struct. 25 (2016), https://doi.org/10.1088/0964-1726/25/4/047001.

[15] G. Zhao, N. Alujević, B. Depraetere, G. Pinte, J. Swevers, P. Sas, Experimental study on active structural acoustic control of rotating machinery using rotating piezo-based inertial actuators, J. Sound Vib. 348 (2015), https://doi.org/10.1016/j.jsv.2015.03.013.

[16] M.J. Brennan, J. Garcia-Bonito, S.J. Elliott, A. David, R.J. Pinnington, Experimental investigation of different actuator technologies for active vibration control, Smart Mater. Struct. 8 (1999) 145–153, https://doi.org/10.1088/0964-1726/8/1/016.

[17] C. Collette, S. Chesné, Robust hybrid mass damper, J. Sound Vib. 375 (2016) 19–27, https://doi.org/10.1016/j.jsv.2016.04.030.

[18] S. Chesné, A. Milhomem, C. Collette, Enhanced Damping of Flexible Structures Using Force Feedback, J. Guid. Control. Dyn. 39 (2016) 1654–1658, https://doi.org/10.2514/1.G001620.

[19] G. Zhao, N. Alujević, B. Depraetere, P. Sas, Dynamic analysis and H_2 optimisation of a piezo-based tuned vibration absorber, J. Intell. Mater. Syst. Struct. 26 (2015), https://doi.org/10.1177/1045389X14546652.

[20] T. Asami, O. Nishihara, Closed-form exact solution to H[sub ∞] optimization of dynamic vibration absorbers (application to different transfer functions and damping systems), J. Vib. Acoust. 125 (2003) 398, https://doi.org/10.1115/1.1569514.

[21] N.W. Hagood, A. von Flotow, Damping of structural vibrations with piezoelectric materials and passive electrical networks, J. Sound Vib. 146 (1991) 243–268, https://doi.org/10.1016/0022-460X(91)90762-9.